Copper and Zinc Promote Interactions between Membrane-Anchored Peptides of the Metal Binding Domain of the Prion Protein†

Angela G. Kenward, Libero J. Bartolotti, and Colin S. Burns*

Department of Chemistry, East Carolina University, Greenville, North Carolina 27858

Received November 30, 2006; Revised Manuscript Received February 2, 2007

ABSTRACT: The prion protein (PrP) has been identified as a metalloprotein capable of binding multiple copper ions and possibly zinc. Recent studies now indicate that prion self-recognition may be an important factor in both the normal function and misfunction of this protein. We have developed fluorescently labeled models of the prion protein that allow prion−prion interactions and metal binding to be investigated on the molecular level. Peptides encompassing the full metal binding region were anchored to the surface of small unilamellar vesicles, and PrP−PrP interactions were monitored by fluorescence spectroscopy as a function of added metal. Both Cu^{2+} and Zn^{2+} were found to cause an increase in the level of PrP−PrP interactions, by 117 and 300%, respectively, whereas other metals such as Ni^{2+}, Co^{2+}, and Ca^{2+} had no effect. The binding of either of these cofactors appears to act as a switch that induces PrP−PrP interactions in a reversible manner. Both glutamine and tryptophan residues, which occur frequently in the metal binding region of PrP, were found to be important in mediating PrP−PrP interactions. Experiments demonstrate that tryptophan residues are also responsible for the low level of PrP−PrP interactions observed in the absence of Cu^{2+} and Zn^{2+}, and this is further supported by molecular modeling. Overall, our results indicate that PrP may be a bifunctional molecule capable of responding to fluctuations in both neuronal Cu^{2+} and Zn^{2+} levels.

The prion protein (PrP)[1] is a cell surface glycoprotein widely expressed in the central nervous system of mammals and avian species (*1*, *2*). The physiological function of PrP, which has yet to be precisely determined, appears to be subtle in nature because PrP-knockout mice exhibit normal development and behavior (*3*). Even close examination of their brain tissue reveals no significant differences compared to that of wild-type mice (*3*), although there is still debate over these studies (*4*−*6*). PrP's direct connection to fatal neurodegenerative diseases, collectively termed transmissible spongiform encephalopathies, has been the impetus for the intense research focus on this protein (*1*, *7*). The normal cellular form of prion is denoted PrP^{C}, and disease results from the refolding of PrP^{C} to the scrapie isoform, termed PrP^{Sc}. Once PrP^{Sc} is generated, it templates the conversion of endogenously expressed PrP^{C} to PrP^{Sc}, causing a buildup of this pathogenic species and, ultimately, neurodegeneration.

It has been the identification of PrP as a copper binding protein that has led to the majority of hypotheses about its normal, cellular function. A major breakthrough was the discovery that Cu^{2+} and Zn^{2+} stimulate the endocytosis of PrP, thus linking metal binding to a physiological response (*8*, *9*). Accordingly, PrP is thought to possess a copper-dependent enzyme function, specifically that of an antioxidant (*5*, *10*), or to participate in copper homeostasis (*8*, *11*, *12*). Other research suggests PrP may be involved in signal transduction (*13*) and cell−cell adhesion (*14*) or function as an anti-apoptosis agent (*15*).

The metal binding region of PrP resides in the flexible N-terminal domain (*4*, *11*, *16*−*18*) and spans residues 60−96 (human sequence). It contains four repeats of the highly conserved octapeptide PHGGGWGQ sequence followed by GGGTH (Figure 1a) (*11*, *16*−*18*). Structural studies have provided precise details about the two types of equatorial Cu^{2+} coordination spheres that exist when PrP is fully loaded with Cu^{2+} (Figure 1b). More recently, studies have begun to provide a picture of the Cu^{2+} coordination modes populated at intermediate and low Cu^{2+} occupancies (*19*, *20*). PrP constructs lacking the metal binding region fail to undergo endocytosis efficiently (*8*, *21*), nor do they exhibit significant antioxidant activity (*10*, *22*). Thus, most of the major copper-dependent responses measured this far are clearly linked to this region.

A number of studies now indicate that PrP self-recognition may be an important factor in both the normal function and misfunction of PrP. Signal transduction was observed upon the antibody-mediated cross-linking of PrP (*13*). Fusion proteins containing N-terminal regions of PrP exhibit self-

† This material is based upon work supported by East Carolina University Research Development Grant Program Award 217305 (C.S.B.), East Carolina University Research/Creative Activity Grant 2004-15 (C.S.B.), and the National Science Foundation via Grant 0521228.

* To whom correspondence should be addressed. Telephone: (252) 328-9790. Fax: (252) 328-6210. E-mail: burnsc@ecu.edu.

[1] Abbreviations: PrP, prion protein; PrP^{C}, cellular isoform of PrP; PrP^{Sc}, scrapie form of PrP; rPrP, recombinant PrP; SHaPrP, Syrian hamster PrP; HuPrP, human PrP; fCJD, familial Creutzfeldt-Jakob disease; SUV, small unilamellar vesicles; DMPC, 1,2-dimyristoyl-*sn*-glycero-3-phosphocholine; PrP(23−28,57−98), residues 23−28 and 57−98 of PrP; GPI, glycophosphatidylinositol; DEPC, diethyl pyrocarbonate; CSF, cerebral spinal fluid; E/M, excimer-to-monomer ratio; GB, generalized Born; MD, molecular dynamics; K_d, dissociation constant; MS, mass spectrometry; rms, root-mean-square distance from the starting structure.

10.1021/bi602473r CCC: $37.00
Published on Web 03/20/2007

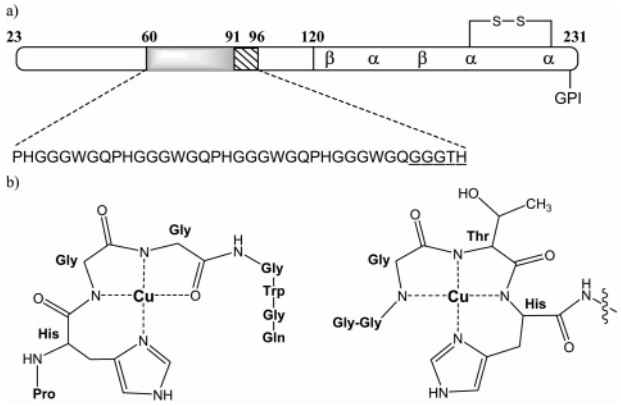

FIGURE 1: Sequence information and structural details of SHaPrP. (a) The metal binding region of PrP resides in the flexible N-terminal domain, and the five main Cu^{2+} binding sites are located in the region of residues 60−96. (b) The structure of a single octarepeat binding site (left) was determined from crystallographic and spectroscopic data. The coordination sphere for residues 91−96, GGGTH (right), is a model based on spectroscopic data.

recognition in a copper- and zinc-dependent manner, but only when the metal binding region is present (*23*). Expansion of this region, which mimics gene inserts associated with familial Creutzfeldt-Jakob disease (fCJD), leads to irreversible multimerization (*23*, *24*). Collectively, these studies suggest that PrP self-recognition is important for the normal function of PrP and that Cu^{2+} and/or Zn^{2+} may be the "switch" that mediates these reversible interactions. Gasset and co-workers have published a series of studies characterizing the amorphous mesh formed by bovine PrP−Cu^{2+} complexes using turbidity, atomic force microscopy, and X-ray absorption spectroscopy (*20*, *25*). They provide evidence of a Cu^{2+} coordination mode involving ligation by two histidine (His) residues. When each His is supplied by a different PrP molecule, Cu^{2+} can act as a bridge between PrPs.

The study presented herein focuses on quantitating the degree of these metal-mediated PrP−PrP interactions and on building a molecular description of PrP self-recognition as a function of Cu^{2+} and Zn^{2+} loading. We have developed an assay based on fluorescence spectroscopy that is capable of providing this information. As the mature form of PrP is tethered to the cell surface by a C-terminal glycophosphatidylinositol (GPI) anchor, the model peptides of the metal binding region used in this study were similarly anchored to the surface of small unilamellar vesicles (SUVs). This strategy serves two important purposes. (1) It aligns the PrP peptides in a parallel fashion as would be found on the cell surface, and (2) it allows for incorporation of the C-terminal fluorophores into the hydrophobic interior of the lipid which is required for the interaction assay. A number of studies have drawn attention to the importance of PrP's cell surface location, especially as this appears to be where PrP^{C} to PrP^{Sc} conversion may take place (*26*−*28*). Although the GPI anchor directs PrP to certain microdomains on the cell membrane, neither it nor the membrane appears to significantly influence the structure of PrP. Studies of rPrP anchored to raftlike liposomes demonstrate that the three-dimensional structure is identical to that of rPrP in solution (*29*, *30*).

Our results show that PrP−PrP interactions are indeed promoted by addition of Cu^{2+} and Zn^{2+}. Interestingly, Zn^{2+} appears to promote these interactions to a much greater degree than Cu^{2+}. Further, through mutation studies, we demonstrate that glutamine (Gln) and tryptophan residues (Trp) play important roles in PrP−PrP interactions. This study advances the understanding of these interactions and thus may provide further insight into the mechanism of endocytosis and the normal physiological function of the prion protein.

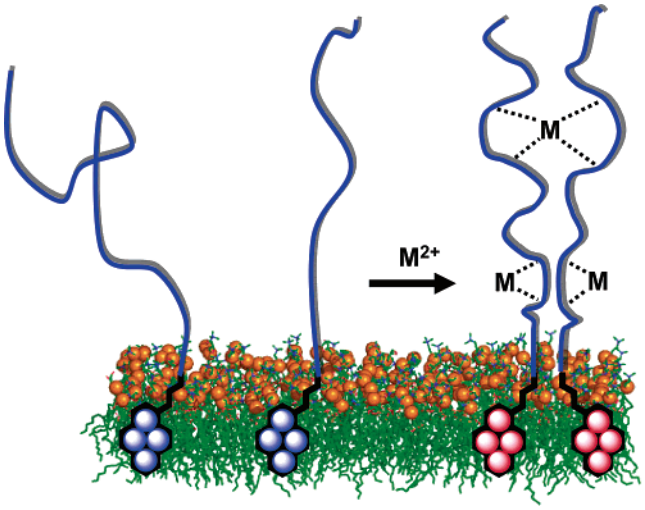

FIGURE 2: General illustration of pyrene-labeled peptides anchored to the outer surface of a SUV. When pyrene fluorophores (colored blue at the left) come into the proximity of one another, they form excimers (colored red at the right) which produce a distinct fluorescence signal at a longer wavelength.

MATERIALS AND METHODS

Synthesis and Purification. All peptides were prepared by solid-phase synthesis using standard fluorenylmethoxycarbonyl (Fmoc) methods. The peptides were all acetylated at the N-terminus and amidated at the C-terminus. The fluorescent molecule 1-pyrenebutyric acid (1-PBA) was purchased from Aldrich (97% pure) and attached via amide bond formation to the side chain of lysine, previously methyltrityl protected, using HBTU, HOBt, and diisopropylethylamine in DMF. Peptides were cleaved from the Rink Amide MBHA resin over a 2 h period using a 95% trifluoroacetic acid/2.5% water/2.5% triisopropylsilane solution (v/v/v). Finally, all peptides were purified by reverse-phase HPLC, using a C18 column, and characterized by electrospray ionization mass spectrometry (ESI-MS) (Bruker Esquire 3000plus quadrupole ion trap).

The molecule 4-pyren-1-yl-*N*-[2-(4-pyren-1-ylbutyrylamino)cyclohexyl]butyramide (Dipyrene; see Figure 3) was synthesized in a one-step reaction by combining 1.92 mmol of (1*R*,2*S*)-1,2-diaminocyclohexane, 3.87 mmol of 1-pyrenebutyric acid, 3.88 mmol of HBTU, and 3.85 mmol of diisopropylethylamine in 25 mL of DMF for 1 h. The molecule was purified by washing with DMF, as it had limited solubility in this solvent whereas all the starting reagents readily dissolve in it, followed by extensive rinses with ethanol. The molecule was characterized by ^{1}H NMR.

Liposome Preparation. For all experiments, small unilamellar vesicle (SUV) liposomes were prepared by making a 0.40 M stock solution of 1,2-dimyristoyl-*sn*-glycero-3-phosphocholine (DMPC) in ethanol (DMPC purchased from Avanti Polar Lipids). A 50 μL aliquot of the DMPC solution

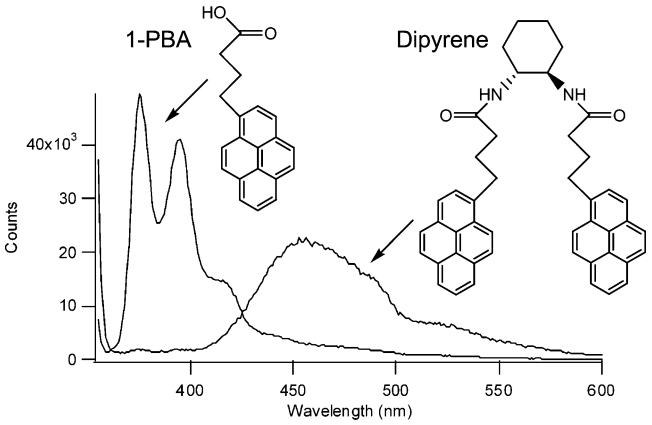

FIGURE 3: Overlay of the fluorescence spectra of 1-PBA and Dipyrene, each at a concentration of 1.55 μM, in a DMPC liposome solution. The spectrum of 1-PBA exhibits maxima at 375 and 395 nm, indicative of noninteracting fluorophores, whereas the broad peak at ~459 nm for Dipyrene is characteristic of excimer formation.

was then added dropwise to 15 mL of a stirring phosphate buffer solution (0.026 M NaH_2PO_4 and 0.041 M Na_2HPO_4 in water) with a pH of 7.25. The mixture was then sonicated at 40 °C for 5 min to produce SUV liposomes (*31*). Peptides were dissolved in dimethyl sulfoxide (DMSO) so that they would remain monomeric in solution, and stock concentrations ranged from 1.0 to 3.0 mM, as determined by the absorbance of the pyrene fluorophore at 345 nm ($\epsilon = 4.3 \times 10^4$ M^{-1} cm^{-1}). High peptide concentrations were necessary to ensure that the final concentration of DMSO was negligible in the liposome solution. Pyrene-labeled peptides, 1-pyrenebutyric acid or Dipyrene, were introduced into the liposome by adding an aliquot of stock solution dropwise to the stirring SUV liposome solution. Addition of pyrene-labeled peptides to solutions of preformed liposomes ensures that the peptides anchor to the outer surface of the liposome. The peptide to liposome molar ratios were less than 1:100.

Fluorescence Spectroscopy. All fluorescence spectra were collected on an ISS PC1 photon counting spectrofluorometer. In all cases, sample volumes of 3.0 mL were placed in a 1.0 cm quartz fluorescence cell for measurement. The sample was excited at 345 nm, and an emission spectrum from 350 to 650 nm was recorded. Titrations were conducted by adding small aliquots (1−5 μL additions) from a $CuSO_4$ solution in 10 mM *N*-ethylmorpholine buffer (pH 7.4). The sample was agitated for approximately 1 min, and the fluorescence spectrum was then recorded. All experiments were performed in triplicate unless otherwise indicated.

The excimer/monomer ratio (E/M) was calculated by integrating the signal intensity from 370 to 429 nm for the monomer contribution and from 430 to 600 nm for the excimer contribution. The E/M ratio of 1-PBA was taken to represent 100% monomer contribution (0% fluorophore interaction), and the E/M ratio of Dipyrene was taken to represent 100% excimer contribution (100% fluorophore interaction). The percent of interacting pyrene fluorophores was calculated using eq 1.

$$\%\ \text{interaction} = [(\text{E/M})_{\text{measured}} - (\text{E/M})_{1-\text{PBA}}]/[(\text{E/M})_{\text{Dipyrene}} - (\text{E/M})_{1-\text{PBA}}] \times 100 \quad (1)$$

where $(\text{E/M})_{1-\text{PBA}} = 0.05 \pm 0.02$ and $(\text{E/M})_{\text{Dipyrene}} = 8.67 \pm 0.01$.

Molecular Dynamic (MD) Modeling Simulations. The generalized Born (GB) model was utilized in the molecular modeling to represent solvation effects. The GB model effectively depicts the electrostatics of molecules in an aqueous environment by representing the solvent as a continuum with the dielectric properties of water, including the charge screening effects of a salt. The main advantage to using the GB model is a significant reduction in the computational time and power required to perform the calculation. The MD modeling consisted of three separate simulations. The first simulation minimized the peptide conformation so that it was in a low-energy form at a temperature of absolute zero. Next, a warming simulation was performed on the minimized conformation that increased the temperature of the system from 0 to 300 K in 6 ps. The final MD simulation was then run until the rms value stabilized, indicating equilibrium within the system, which was on the order of several nanoseconds. The MD simulations were performed with AMBER (*32*) on an SGI Origin 350 workstation.

RESULTS

PrP Model Peptide and Metal Effects. We have synthesized PrP peptides that contain fluorescent lipophilic anchors covalently attached at their C-termini. When incorporated on the outer surface of liposomes, these model peptides allow PrP−PrP interactions to be probed as a function of added metal. Further, these peptides are synthesized, so the role of single residues is easily explored through mutation. The fluorescence assay is based on the proximity of pyrene fluorophores, which are located inside the lipid bilayer (Figure 2). When two pyrene molecules are close in space, they form an excimer species which has an emission spectrum distinct from that of monomeric pyrene. The ratio of the excimer signal to the monomer signal provides a means of quantitating the level of interactions.

The excimer/monomer ratio (E/M), which was calculated by integrating the signal intensity from 370 to 429 nm for the monomer contribution and from 430 to 600 nm for the excimer contribution, helps to illustrate the degree of interaction in a quantitative manner. Using the model compounds 1-pyrenebutyric acid (1-PBA) and Dipyrene, a scale corresponding to percent fluorophore interaction was developed. Figure 3 shows the overlaid fluorescence spectra of these two compounds in DMPC liposomes. At low concentrations (<100 μM), the E/M ratio of 1-PBA was taken to represent 100% monomer contribution and thus 0% fluorophore interaction. Similarly, the E/M ratio of Dipyrene was taken to represent 100% excimer contribution and thus 100% fluorophore interaction.

The model peptide of the metal binding region of PrP is shown in Figure 4 (and Table 1) and is termed the native PrP model. It also contains the KKRPKP solubilizing sequence at the N-terminus, corresponding to residues 23−28, and glycine spacers at the C-terminus surrounding the lysine-linked pyrene anchor. The glycine spacers were added to increase the synthetic yield of the peptide and to provide sufficient distance between the lipophilic anchor and metal binding region. Peptides like this, albeit without the pyrene fluorophore, have been shown to bind copper in a manner consistent with that observed for the full-length protein

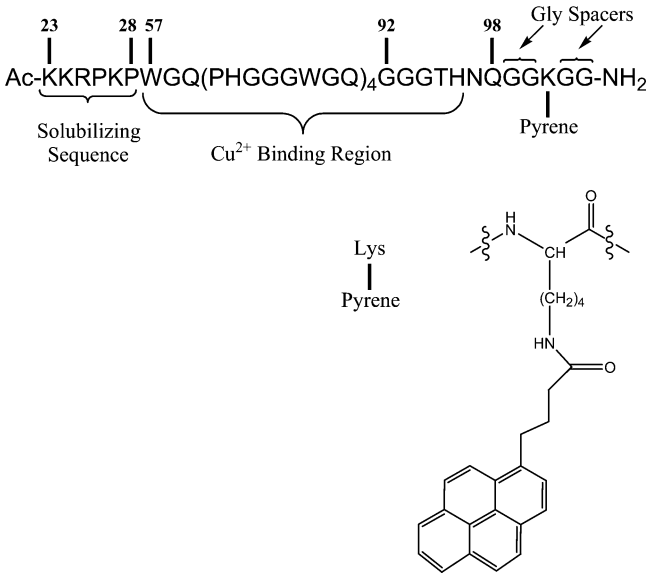

FIGURE 4: Composition and details of the peptide model of PrP's metal binding region. The pyrene fluorophore was linked to the side chain of a C-terminal lysine.

Table 1: PrP-Derived Peptide Sequences[a]

Native	Ac-KKRPKPWGQPHGGGWGQPHGGGWGQPHGGGWGQPHGGGWGQGGGTHNQGGK(Pyr)GG-NH$_2$
Gln→Ala	Ac-KKRPKPWG**A**PHGGGWG**A**PHGGGWG**A**PHGGGWG**A**PHGGGWG**A**GGGTHN**A**GGK(Pyr)GG-NH$_2$
Trp→Ala	Ac-KKRPKP**A**GQPHGGG**A**GQPHGGG**A**GQPHGGG**A**GQPHGGG**A**GQGGGTHNQGGK(Pyr)GG-NH$_2$
Trp73→Ala	Ac-KKRPKPWGQPHGGGWGQPHGGG**A**GQPHGGGWGQPHGGGWGQGGGTHNQGGK(Pyr)GG-NH$_2$
OR2	Ac-PHGGGWGQPHGGGWGQGGGTHNQGGK(Pyr)GG-NH$_2$

[a] All peptides contain a pyrene (Pyr) fluorophore attached to the side chain of a C-terminal lysine.

(see Figure 1) (*16*−*18*). The fact that PrP−PrP interactions have been observed between fusion proteins containing the octarepeat region (residues 60−91) and between full-length rPrPs indicates that study of the metal binding region itself should provide meaningful information about the nature of these interactions (*20*, *23*, *25*).

A series of quenching experiments were undertaken to ensure that the pyrene fluorophore was being incorporated into the liposomes. First, the lipid soluble quencher bromobenzene (BB) was added during preparation of the liposomes. When a concentration of 240 μM bromobenzene was used (which yielded an 18:100 BB:DMPC molar ratio), the total fluorescence intensity was reduced by approximately 55% for the native peptide system and for 1-pyrenebutyric acid itself. Further quenching was not achieved because increasing the BB concentration disrupted the liposomes. The fact that a lipid soluble quencher is effective at quenching a large percentage of the fluorescence intensity indicates that a high percentage of the pyrene moieties is incorporated into liposomes. If a significant amount of the pyrene fluorophore was partitioning into another lipophilic environment, e.g., if the peptide folded upon itself to provide a hydrophobic interior, then the BB would not be present there to cause quenching, and one would expect a more intense fluorescence signal.

Almost no fluorescence signal was observed when the pyrene-labeled peptides were prepared without DMPC. Thus,

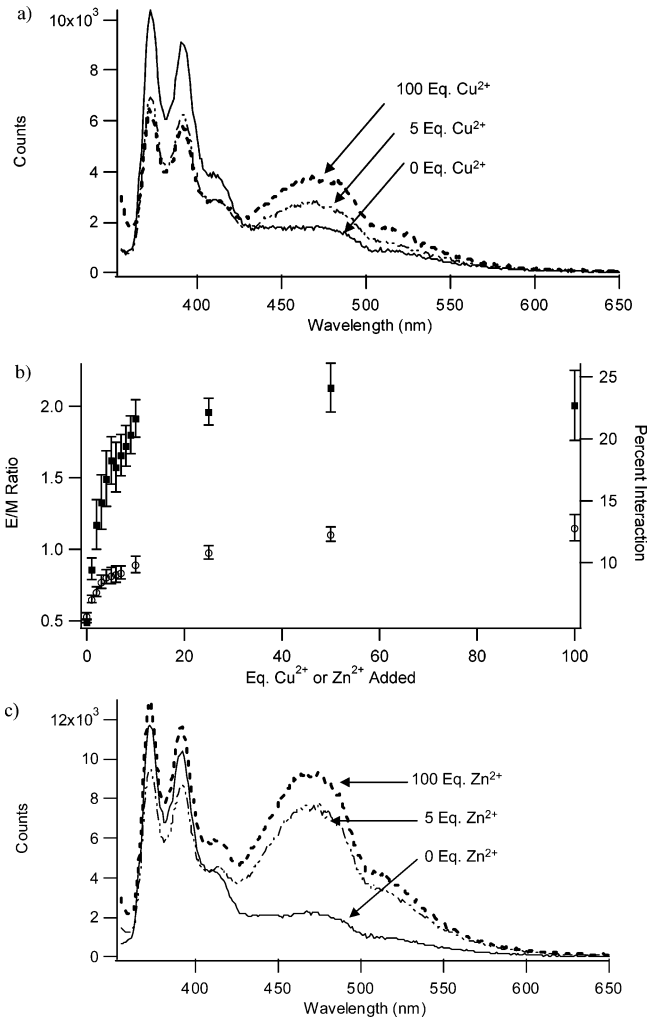

FIGURE 5: (a) Fluorescence spectra of the native PrP peptide (4.15 μM) at three different Cu^{2+} loadings in a liposomal solution. (b) E/M ratio for the native PrP peptide as a function of titrated Cu^{2+} (○) and Zn^{2+} (■). (c) Fluorescence spectra of the native PrP peptide (4.26 μM) at three different Zn^{2+} loadings in a liposomal solution. The percent of interacting fluorophores presented at the right, *y*-axis, was calculated using eq 1. The metal ion concentration is reported in equivalents per peptide. Error bars represent one standard deviation.

it can be concluded that any of the fluorophore not incorporated into the liposome does not produce a fluorescent signal. The Cu^{2+} titration of the native PrP model (Figure 5a) shows that exposure to metal does not cause significant dissociation of the pyrene moiety from the liposome because a significant reduction in fluorescence intensity would have been observed. In all cases, the fluorescent counts, as measured by integration of the entire spectrum, at 100 equiv of Cu^{2+} were within ±10% of the counts at 0 equiv of Cu^{2+}. Last, to ensure that the pyrene-labeled peptides did not self-associate over extended time periods, a time dependence study was conducted. The E/M ratio of the native PrP model in liposome solution showed little variation over a 4 h period, which corresponds to the length of time for a single complete titration experiment.

Figure 5a displays the fluorescence spectrum of the native PrP model in the liposomal system at pH 7.25. Visual examination of the spectrum reveals the presence of a low-intensity excimer peak at 0 equiv of added Cu^{2+}. The concentration of the peptide was 4.15 μM, which in control experiments with 1-pyrenebutyric acid and control peptides

Table 2: E/M Ratios and Percent Interaction for PrP-Derived Peptides

peptide and metal	$(E/M)_{initial}$	$(E/M)_{final}$	% of peptides interacting	
			initial	final
native PrP and Cu	0.53 ± 0.02	1.15 ± 0.09	5.6 ± 0.5	13 ± 1
native PrP and Zn	0.50 ± 0.02	2.0 ± 0.3	5.2 ± 0.3	23 ± 3
Gln → Ala PrP and Cu	0.41 ± 0.04	0.76 ± 0.03	4.2 ± 0.5	8.2 ± 0.4
Gln → Ala PrP and Zn	0.42 ± 0.04	0.92 ± 0.09	4.2 ± 0.5	10 ± 1
Trp → Ala PrP and Cu	0.05 ± 0.01	0.27 ± 0.01	0.03 ± 0.02	2.6 ± 0.3
Trp → Ala PrP and Zn	0.05 ± 0.03	0.63 ± 0.03	0.03 ± 0.02	6.7 ± 0.4
OR2 PrP and Cu	0.38 ± 0.03	0.65 ± 0.03	3.8 ± 0.4	6.9 ± 0.4
OR2 PrP and Zn	0.26 ± 0.07	1.46 ± 0.07	2.4 ± 0.8	16.4 ± 0.9
Trp73 → Ala PrP	0.34 ± 0.01	−	3.4 ± 0.3	−

was well below the threshold at which pyrene concentration alone could account for excimer formation. Thus, we conclude these peptides interact with each other to a small degree in the absence of metal. Point mutation studies, which will be discussed below, further serve to support this conclusion.

When copper is titrated into the peptide/liposome solution, the excimer peak grows in intensity with a concomitant decrease in the magnitude of the monomer peak (Figure 5a). A plot of the E/M ratios versus the number of equivalents of copper added is shown in Figure 5b. Overall, addition of Cu^{2+} increases the E/M ratio from 0.53 ± 0.02 to 1.15 ± 0.09, which represents a 117% change. Alternatively, this can be viewed in terms of the percent of interacting peptides, with an initial value of 5.6% in the absence of Cu^{2+} and reaching 13% at 100 equiv of Cu^{2+}. The half-maximal effect is reached at approximately 8 equiv of added Cu^{2+}. These data suggest that Cu^{2+} does in fact promote interactions between PrP molecules. The effect observed here is also reversible; for instance, when the metal chelator histidine is added in an amount equivalent to the copper concentration, the magnitude of the excimer peak is reduced to its pre-copper-loaded value (i.e., E/M = 0.53 ± 0.02; see Table 2 for all E/M values and percent interactions). Addition of glycine was also effective, but a higher concentration was necessary to reduce the intensity of the excimer peak (data not shown).

Addition of zinc to the peptide/liposome solution produces an effect similar to that of copper, although it is more pronounced (Figure 5b,c). Addition of Zn^{2+} increases the E/M ratio from 0.50 ± 0.02 to 2.0 ± 0.3, representing a 300% change. At 100 equiv of added Zn^{2+}, 23% of the peptides are interacting. The half-maximal effect is reached around 3.0 equiv of added Zn^{2+}, and there is clearly a saturation point at 10 equiv of Zn^{2+}. These results suggest that Zn^{2+} is more effective at bringing fluorophores close together and thus promoting PrP−PrP interactions more effectively.

Other divalent metals such as Ni^{2+}, Co^{2+}, and Ca^{2+} did not cause excimer formation; as an example, the titration of the native PrP peptide with Co^{2+} is shown in Figure 6. This demonstrates that the effect being observed is specifically promoted by Cu^{2+} and Zn^{2+}.

Exploring Residues Responsible for PrP−PrP Interactions. Model peptides with point mutations were synthesized to explore the residues responsible for the metal-induced PrP−PrP interactions and to gain a better understanding of the types of interactions between peptides. Given the repetitive nature of the metal binding region of PrP, our initial approach

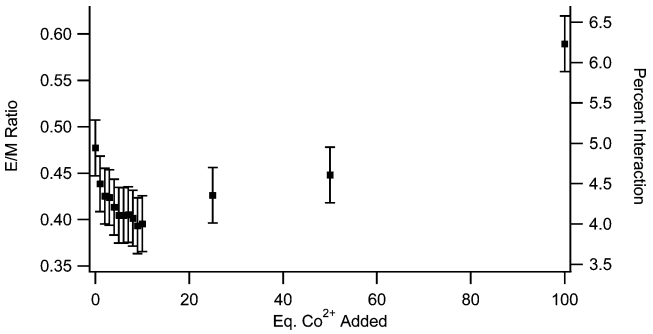

FIGURE 6: E/M ratio for the native PrP peptide (4.78 μM) as a function of titrated Co^{2+}. This experiment was performed in duplicate, and error bars represent 10% of the largest E/M value measured.

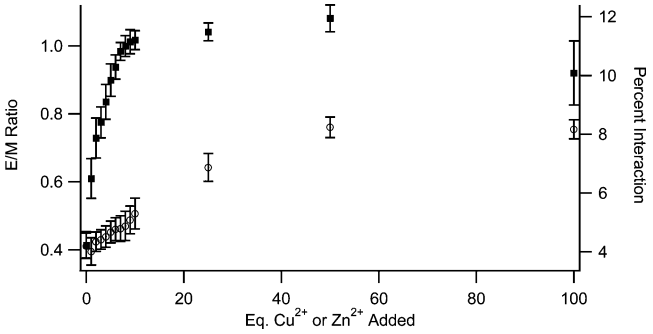

FIGURE 7: E/M ratio for the Gln → Ala PrP peptide (4.66 μM) as a function of titrated Cu^{2+} (○) and Zn^{2+} (■). Error bars represent one standard deviation.

involved the complete mutation of one residue type with alanine. We selected Gln and Trp as the residues to mutate because they possess functionalized side chains and are not essential for directly coordinating Cu^{2+} or Zn^{2+} (*11*). The constitutions of the Gln → Ala and Trp → Ala peptides are listed in Table 1.

Binding studies have shown that glutamine is not necessary for Cu^{2+} coordination by PrP. This, in conjunction with the fact these Gln residues are highly conserved in mammalian prions (*2*), led to the hypothesis that they facilitate intermolecular interactions between neighboring, membrane-anchored PrPs (*11*). Figure 7 displays the E/M ratio for the Cu^{2+} titration of the Gln → Ala peptide. Although the initial E/M ratio of 0.41 ± 0.04 was close to that of the native PrP model (E/M = 0.53 ± 0.02), the growth of the excimer peak as a function of added Cu^{2+} was noticeably different. Overall, addition of Cu^{2+} increases the E/M ratio from 0.41 ± 0.04 to 0.76 ± 0.03, a change of 85%, and the half-maximal effect was reached at approximately 20 equiv of added Cu^{2+}. From these data, it can be concluded that the Gln residues play a role in mediating Cu^{2+}-induced PrP−PrP interactions. The effect of the Gln mutation is more subtle in the case of Zn^{2+}-promoted interactions, as shown in Figure 7. This titration curve follows the same trend as that of the native PrP model, with an apparent foldover point at 10 equiv of added Zn^{2+} and a half-maximal effect at approximately 3 equiv of added Zn^{2+}. The major difference was found in the overall change in the E/M ratio from 0.42 ± 0.04 to 0.92 ± 0.09, which is a 119% change.

The second residue that was examined was tryptophan. The metal binding region of PrP has a high frequency of Trp residues, a residue which is also highly conserved across

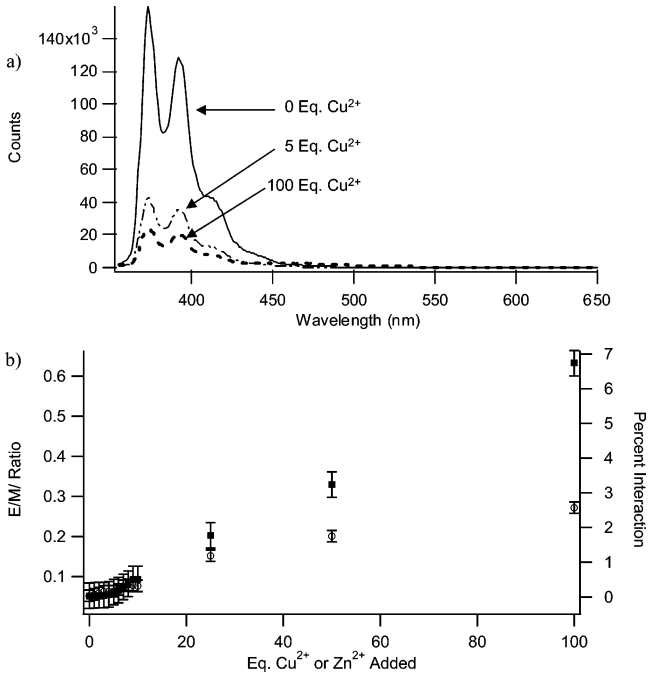

FIGURE 8: (a) Fluorescence spectra of the Trp → Ala PrP peptide (4.51 μM) at three different Cu^{2+} loadings. (b) E/M ratio for the Trp → Ala PrP peptide (4.51 μM) as a function of titrated Cu^{2+} (○) and Zn^{2+} (■). This experiment was performed in duplicate, and error bars represent 10% of the largest E/M value measured.

mammalian prions (*2*). The crystal structure of the HGGGW−Cu^{2+} complex reveals that Trp may participate in Cu^{2+} coordination, although in a peripheral manner. The nitrogen of the indole side chain may participate in a hydrogen bond with the oxygen of an axially bound water. The fluorescence spectra of the Trp → Ala model as a function of added Cu^{2+} are noticeably different from those of the native PrP model (Figure 8a). First, the photon counts are much higher; in fact, they are the same as those observed for an equal concentration of 1-pyrenebutyric acid incorporated into a liposome. It appears this peptide incorporates itself into the liposome in such a way that the pyrene is less effectively quenched, perhaps due to deeper penetration into the lipid membrane. Again, incorporation of BB reduced the fluorescence intensity in the expected manner, ensuring the pyrene is incorporated into the liposome. Second, there is no evidence of an initial excimer peak in the absence of added metal. The E/M of 0.052 ± 0.02 is similar to that of 1-pyrenebutyric acid (E/M = 0.050 ± 0.02). This feature was particularly interesting, and this will be addressed further in the following section. As Cu^{2+} was added, the counts reduced dramatically (at 100 equiv of Cu^{2+}, the counts were 20% of their initial value at 0 equiv of Cu^{2+}), and an excimer peak grew in intensity. We hypothesize that metal binding reorganizes the peptide, causing the pyrene to relocate closer to the liposome−water interface. Normalizing the most intense peak at 372 nm allows the excimer formation to be seen (data not shown). The titration plot (Figure 8b) shows an overall increase in the E/M ratio as a function of added Cu^{2+}. Prior to the addition of Cu^{2+}, there are almost no peptide−peptide interactions, as E/M = 0.03 ± 0.02, and at 100 equiv of added Cu^{2+}, this value grows to an E/M of 0.27 ± 0.01, which means only 2.6% of the peptides are interacting at this high Cu^{2+} load.

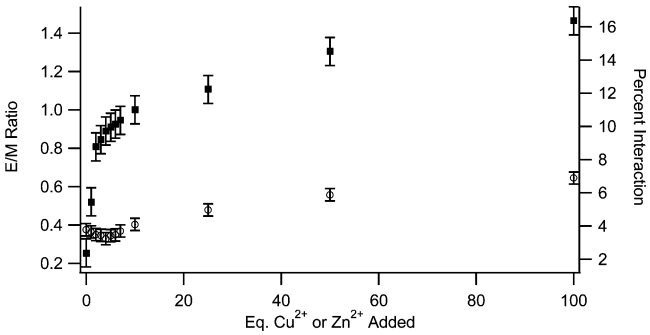

FIGURE 9: E/M ratio for the OR2 peptide (3.61 μM) as a function of titrated Cu^{2+} and Zn^{2+}. This experiment was performed in duplicate, and error bars represent 10% of the largest E/M value measured.

The Zn^{2+} titration was similar to that with Cu^{2+}, but no change in the E/M ratio was observed until 4 equiv of Zn^{2+} was added (Figure 8b). Addition of Zn^{2+} increased the E/M ratio from 0.05 ± 0.03 to 0.63 ± 0.03. Again, prior to the addition of Zn^{2+}, almost no peptide interactions are present. At 100 equiv of Zn^{2+}, only 6.7% of the peptides are interacting. Overall, this model peptide behaves in a manner very different from that of the native PrP model.

Truncated Models of PrP's Metal Binding Region. The repetitive nature of the metal binding sequence led us to question whether the metal-dependent interactions required the full metal binding region or whether it could function in a segmental manner. To explore whether smaller segments could promote PrP−PrP interactions, albeit to a lesser degree, we synthesized the OR2 model peptide (Table 1). This peptide spans residues 76−98 and contains two octarepeats and the GGGTH binding site. A plot of the E/M ratios versus the equivalents of copper added is shown in Figure 9. Overall, addition of Cu^{2+} increases the E/M ratios from 0.38 ± 0.03 to 0.65 ± 0.03, a change of 71%, and the half-maximal effect is reached at approximately 34 equiv of added Cu^{2+}. Again, the titration with Zn^{2+} is noticeably different, where addition of the metal increases the E/M ratio by 462% (from an E/M of 0.26 ± 0.07 to 1.46 ± 0.07), and the half-maximal effect is reached at approximately 4.9 equiv (Figure 9). This very large percent change is due to the low level of peptides initially interacting (i.e., 2.4% prior to addition of Zn^{2+}).

Computational Studies of PrP−PrP Interactions in the Absence of Added Cu^{2+} and Zn^{2+}. The metal free fluorescence spectrum of the Trp → Ala model showed no excimer peak, indicating that Trp is necessary for PrP−PrP interactions in the absence of metal. We hypothesize that the Trp residues may be interacting either in a hydrophobic manner or by $\pi-\pi$ interactions. To explore this, we performed molecular dynamic (MD) modeling simulations. The generalized Born (GB) model was utilized for the molecular modeling to represent solvation effects. The sequence shown in the caption of Figure 10 was used for molecular dynamic simulations, and it encompasses the full-length PrP metal binding region. The initial starting coordinates for the model were taken from a NMR structure of HuPrP(61−84) containing three octarepeat units (PDB entry 1OEI) (*33*). The remaining octarepeat and GGGTH binding site were then added to this file along with the solubilizing sequence. It should be noted that the molecular modeling was performed on peptides in free solution and not anchored to a membrane.

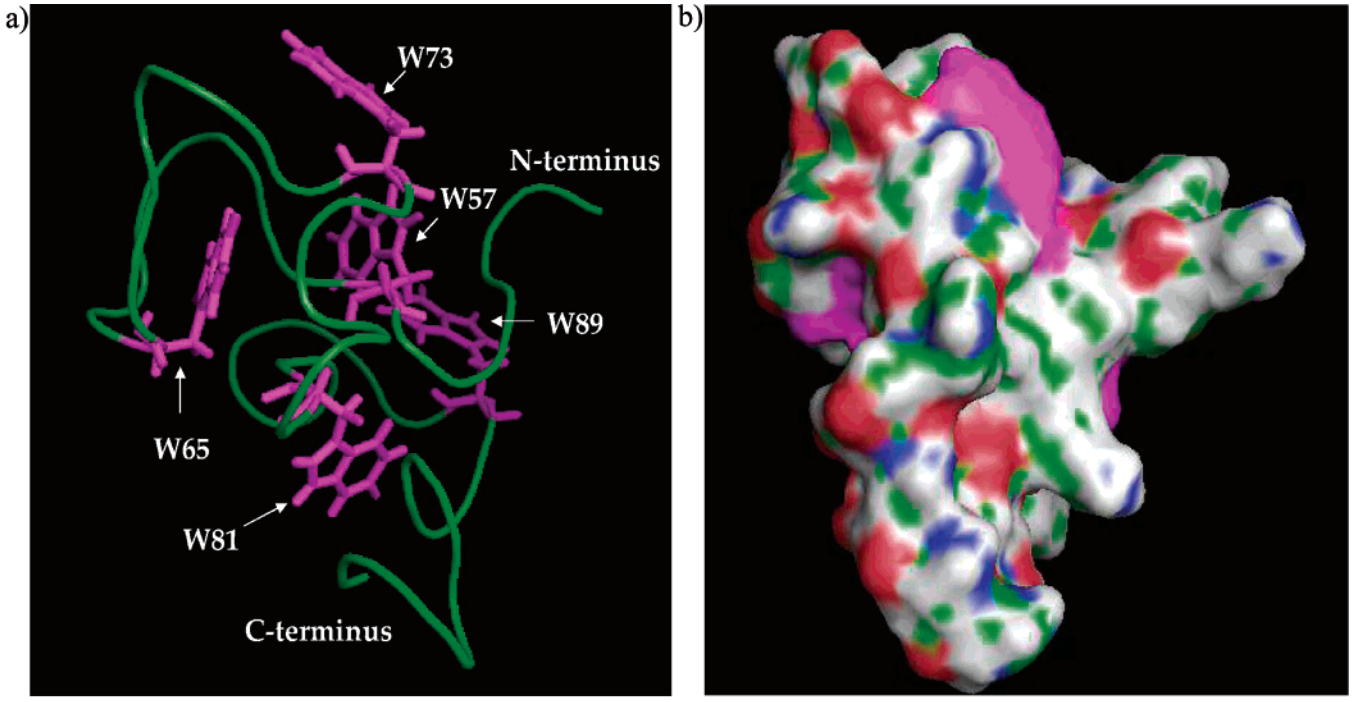

FIGURE 10: Generalized Born model of the equilibrated PrP peptide. (a) Three-dimensional rendering and (b) surface potential diagram. Tryptophan residues are highlighted in purple. The peptide sequence and numbering system used for computations is illustrated below.

57 65 74 81 89
Ac-KKRPKPWGQPHGGGWGQPHGGGWGQPHGGGWGQPHGGGWGQGGGTHNQGGG-NH_2

The purpose of these modeling studies is to provide the first step in exploring the feasibility of intermolecular Trp−Trp interactions between PrPs via their metal binding region.

Panels a and b of Figure 10 display the equilibrated GB model of the PrP model peptide as a ribbon model and the surface potential diagram, respectively. In Figure 10a, we notice that the C-terminus extends away from the rest of the peptide, a conformation that could allow the pyrene fluorophore to extend into a liposome. The solubilizing sequence at the N-terminus of the peptide model extends away from the copper-coordinating region. Interestingly, one of the Trp residues (Trp73) is exposed to the water potential as illustrated in the surface potential diagram of PrP. Because tryptophan possesses a hydrophobic side chain, one would expect all the indole rings to be shielded from the hydrophilic environment by clustering inside of the peptide. The suggestion that Trp73 may be solvent-exposed led us to hypothesize that a Trp73−Trp73 interaction may be responsible for the self-association in the absence of metal. Again we used MD modeling to address this possibility.

A dimer was constructed by bringing two PrP molecules together so that the Trp73 residues stacked in a face to face manner. This dimer model served as a starting point for MD calculations, and the simulation ran for 3 ns before reaching equilibrium. The starting and final MD structures are shown in panels a and b of Figure 11, respectively. Two noteworthy points from this simulation are (1) the dimer remained intact and (2) a number of Trp residues migrated close to one another, forming what appears to be a hydrophobic cluster. These simulations provided the basis for synthesizing and testing the Trp73 → Ala model peptide, the fluorescence spectrum of which is shown in Figure 12. An excimer peak is still present in this case, but the E/M of 0.34 ± 0.01 is noticeably lower than that of the native peptide model where E/M = 0.53 ± 0.02. This finding strongly suggests that Trp residues might be important for low-level PrP−PrP interactions that facilitate PrP clustering.

DISCUSSION

The findings reported here demonstrate that both Cu^{2+} and Zn^{2+} promote interactions between the metal binding regions of PrP molecules (Figure 5), as modeled by the C-terminally pyrene-anchored PrP(23−28,57−98) peptide. These interactions are reversible because addition of chelators reduces the E/M ratio to its original metal-free value. Further, these interactions are specific to Cu^{2+} and Zn^{2+} because other divalent cations did not increase the E/M ratio significantly. Together, these results bear a striking parallel to cell studies showing that only Cu^{2+} and Zn^{2+} stimulate endocytosis (*9*) and to oligomerization studies demonstrating the involvement of metal ions (*20*, *23*, *25*).

It is particularly notable that Zn^{2+} promotes PrP−PrP interactions more effectively and to a much greater extent than Cu^{2+} (23 and 13%, respectively). A number of studies have examined the metal binding affinity of PrP for metals other than Cu^{2+}, and the general conclusion is that Zn^{2+} bound weakly. Although Qin et al. (*16*) were unable to directly detect any Zn^{2+}-bound forms of HuPrP23−98 using MALDI-MS, they did find that addition of Zn^{2+} protects one or two histidine residues from diethyl pyrocarbonate (DEPC) modification, in contrast to the five protected by Cu^{2+}. Working with PrP57−91, Whittal et al. observed Zn^{2+} binding by ESI-MS and concluded that the K_d exceeds 25 μM (*34*). None of the mass spectrometry studies report detection of peptide oligomerization caused by the addition of Zn^{2+}. This may be explained, in part, by the fact that the MS studies were performed on peptide solutions, whereas

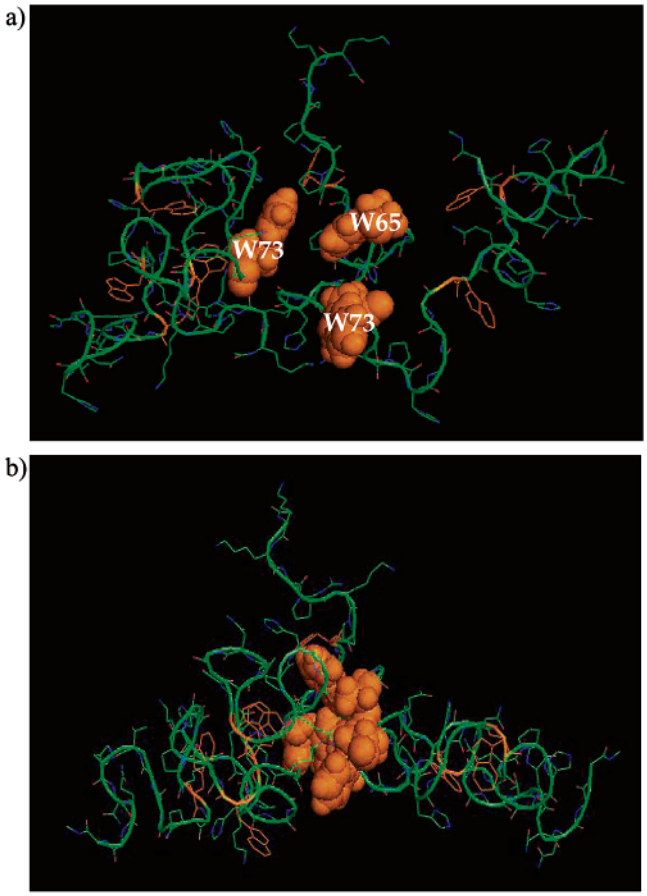

FIGURE 11: Generalized Born model of a PrP−PrP dimer. (a) Starting structure for GB molecular modeling of a PrP dimer based on interaction between Trp73 of each peptide. (b) Equilibrated GB structure. Trp residues are highlighted in orange, and three indole side chains (Trp73 being the left molecule and Trp65 and Trp73 the right molecule) are displayed as space filling representations.

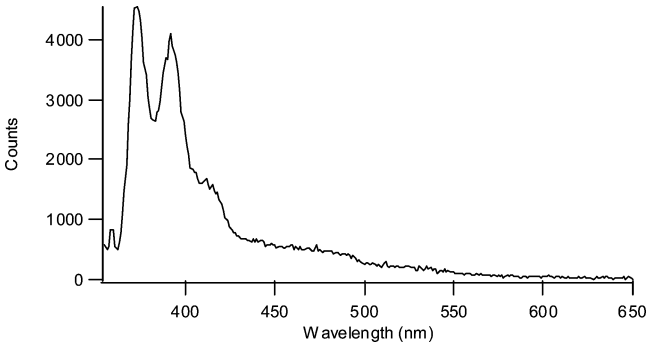

FIGURE 12: Fluorescence spectrum of the Trp73 → Ala PrP peptide (3.10 μM) in a liposomal solution.

this study used liposome-anchored peptides, which should better approximate in vivo conditions. Further, the interactions responsible for oligomer formation may be disrupted by the desolvation conditions encountered in the MS experiment. Jackson et al. report that the Zn^{2+} binding affinities of both HuPrP91−231 and HuPrP52−98 are several orders of magnitude weaker than for Cu^{2+}, although the absolute K_d values they determined are unusually low and far outside the range most other studies report (*35*). Despite the finding that PrP's affinity for Zn^{2+} appears to be very weak, the fact that other divalent metals, especially Co^{2+}, were unable to promote PrP−PrP interactions leads us to conclude that membrane-anchored PrP does indeed specifically bind Zn^{2+}.

The hypothesis that PrP is involved in neuronal zinc homeostasis has already been put forth on the basis of the observations that Zn^{2+} stimulates PrP endocytosis and the levels of Zn^{2+} present in the brain are very high (*36*). The zinc concentration is much higher in the brain parenchyma than that of copper, with one report of 350 μM Zn^{2+} versus 70 μM Cu^{2+} (*37*). Other researchers have reported measuring similar Zn^{2+} concentrations for wet brain tissue (*38*). It is difficult to specify the extracellular Zn^{2+} concentration, but if the Zn^{2+} concentration of the cerebral spinal fluid (CSF) is taken to represent the extracellular Zn^{2+} concentration, then it is in the nanomolar range (*39*, *40*). It is unlikely that PrP could successfully compete for Zn^{2+} at concentrations below the tens of micromolar range. However, at the peak of stimulated neuronal activity, the concentration of Zn^{2+} released into the extracellular space has been reported to reach as high as 300 μM (*41*). This concentration is within the range used by Harris to stimulate endocytosis in PrP-expressing N2a mouse neuroblastoma cells (100−500 μM) (*8*). Therefore, the interaction of PrP with Zn^{2+}, which promotes PrP−PrP interactions, is potentially relevant from a physiological standpoint. Our findings here also support similar arguments for PrP's involvement in Cu^{2+} homeostasis (*8*, *11*, *12*). It appears PrP may be a bifunctional molecule capable of responding to fluctuations in both neuronal Cu^{2+} and Zn^{2+} levels.

Differentiation between the formation of dimeric species and higher-order multimeric species is not possible using the method to detect peptide−peptide interactions, i.e., the proximity of pyrene fluorophores and their ability to form excimer complexes. At a minimum, we can conclude at least dimers form, but the results of other researchers strongly suggest that PrP interacts in such a way that they form higher-order multimeric species (*20*, *23*, *25*). The nature of the Cu^{2+}-induced PrP−PrP interaction has been investigated in depth by Gasset and co-workers (*20*). Using X-ray absorption spectra of BoPrP(24−242) and numerous octarepeat peptide models, they concluded that at half-site occupancy the Cu^{2+} coordination sphere consisted of four equatorial nitrogens, two from histidine imidazole rings and two from deprotonated glycine amides. From this, they proposed that the coordination of a single Cu^{2+} by two histidine residues, each provided by a different PrP molecule, constitutes the mechanism of PrP cross-linking. The existence of different coordination modes as a function of Cu^{2+} occupancy has been further investigated by Chattopadhyay et al. (*19*). Similarly, they provide evidence of the coordination of a single Cu^{2+} by two or more His imidazoles at intermediate Cu^{2+} occupancy. As the Cu^{2+} load is increased, ultimately resulting in full Cu^{2+} occupancy, the coordination mode of the octarepeat unit changes such that a pentacoordinate complex forms involving the specific HGGGW residues (*11*, *18*). At this point, each octarepeat histidine coordinates a single Cu^{2+} (*11*, *18*−*20*). This binding mode does not support metal cross-linking via coordination of multiple His residues. Given that we observe that the frequency of PrP−PrP interactions to increase as a function of added Cu^{2+} or Zn^{2+}, at levels where full saturation is expected, suggests that either the binding mode characterized at low and intermediate Cu^{2+} loads persists at or near full Cu^{2+} saturation, a finding in line with Chattopadhyay et al.'s work, or another cross-linking mechanism is operative. Since we

have yet to spectroscopically characterize the Cu^{2+}-bound forms of the pyrene-anchored PrP molecules in their liposomal environment, the possibility that the coordination mode, or population of coordination modes, differs from that observed in solutions without liposomes exists. Both the truncated PrPs and those with point mutations, discussed below, will serve to help resolve the mechanism of metal-mediated PrP cross-linking.

Direct structural investigation of binding of Zn^{2+} to PrP is complicated by the fact it is a d^{10} metal which is EPR silent and NMR inactive. Thus, it eludes direct detection by both electronic and magnetic resonance spectroscopy. Even though structural information about PrP−Zn^{2+} binding is lacking, it is likely that the mechanism of PrP−PrP interaction promoted by Zn^{2+} involves multiple-His coordination from different PrP molecules. The majority of Zn^{2+} binding proteins make use of the imidazole nitrogen of histidine, the carboxyl group of glutamic acid (Glu), and the sulfhydryl group of cysteine (Cys) as ligands (*42*, *43*). Since PrP's metal binding region lacks all of these residues except His, and given that Zn^{2+} is not widely reported to bind to deprotonated amide nitrogens as Cu^{2+} does, His is the only reasonable candidate as a ligand. Again, the truncated PrPs and those with point mutations will serve to help resolve the mechanism of Zn^{2+}-mediated PrP cross-linking.

The OR2 peptide, which contains two octarepeats plus the GGGTH binding site, serves to answer the question of whether the metal-dependent interactions require the full metal binding region. In the case of Cu^{2+} addition, the titration curve significantly deviates from that of the corresponding native PrP model. The percent of PrP−PrP interactions at first decreases as a function of added Cu^{2+}, and at the end point, the overall percent interaction is 6.9% versus 13% for the native PrP model. Interestingly, the OR2 model does interact with itself in a Cu^{2+}-dependent manner, although the maximum degree of interaction has been reduced by close to 50% (when compared to that of the native peptide). Thus, the full octarepeat region is needed for normal titration behavior, but not a requirement for interactions to occur. It is interesting to note that the percent interaction appears to scale with the number of octarepeat units (note, the native PrP peptide has four octarepeat units). The behavior of OR2 as a function of Zn^{2+} is remarkably similar to that of the native PrP model, the only difference being that the amount of Zn^{2+} needed to produce the half-maximal effect has increased by 40% and the overall percent interaction has decreased by 40%. These numbers appear to scale with the total number of binding units or His residues, of which the native PrP peptide has five.

Previously, it has been proposed that the Gln side chains of the metal binding region facilitate intermolecular recognition between neighboring PrPs. Both Gln and Asn rich regions are thought to participate in regulatory processes through protein−protein contacts (*44*). Glutamine residues are also key components in the formation of "polar zippers", which are β-sheets strengthened by side chain hydrogen bonding interactions (*45*). Interestingly, a number of neurodegenerative diseases are linked to abnormally expanded glutamine repeats (*46*). The Cu^{2+} titration of the Gln → Ala peptide demonstrates the importance of this residue in PrP−PrP interactions. Addition of a much greater amount of Cu^{2+} to this mutant is required before a significant increase in the level of interactions occurs. Despite the absence of Gln, Cu^{2+} is still able to promote PrP−PrP interactions but to a lesser degree (36% less compared to the native PrP model). On the other hand, the behavior of the Gln → Ala peptide as a function of Zn^{2+} is notably similar to that of the native PrP model. The amount of Zn^{2+} needed to produce the half-maximal effect is essentially unchanged, even though the overall percent interaction has decreased by 50%. Overall, Gln plays a very important role in PrP−PrP interactions, especially those promoted by Cu^{2+}, but another cross-linking mechanism must also be operative. Two ways can be envisioned by which Gln can facilitate PrP−PrP interactions. (1) It forms H-bonds, very likely to another Gln residue, or (2) it exerts a steric effect given the restricted rotation of its ϕ and ψ angles.

The mutation of the Trp residues, as assessed by the Trp → Ala peptide, had a profound effect on not only the metal-induced interactions but also the amount of PrPs associating in the absence of metal. The Cu^{2+} and Zn^{2+} titration behavior of the Trp → Ala peptide was significantly altered from that of the native PrP model, with only minimal increases in the percent of interactions. The photon counts observed for this peptide are much higher than for any other peptide system that has been studied; in fact, they are the same as observed for an equal concentration of 1-pyrenebutyric acid incorporated into a liposome. It appears this peptide incorporates itself into the liposome in such a way that the pyrene anchor is located deeper inside. As Cu^{2+} was added, the counts were reduced dramatically (at 100 equiv of Cu^{2+}, the counts were 20% of their initial value at 0 equiv of Cu^{2+}), and an excimer peak grew in intensity. We hypothesize that metal binding reorganizes the peptide, causing the pyrene to relocate closer to the liposome−water interface. Since this system behaved differently than the others, it is difficult to completely separate the effects of the altered membrane anchoring from Trp's influence on PrP−PrP cross-linking. Although it is possible that Trp−Trp interactions provide the mechanism of cross-linking, to a lesser degree without metal and to a greater degree with metal bound, it is also possible that substitution of the Trp residues alters PrP's metal binding modes and affinities. Zahn finds that the HGGGW segment of each octarepeat exists in a "loop" conformation at physiological pH (*33*). This HGGGW loop conformation has a backbone fold similar to that observed in the HGGGW−Cu^{2+} crystal structure. Disruption of the apparently preorganized binding site may lower the Cu^{2+} binding affinity and/or promote the population of a coordination mode that does not facilitate PrP−PrP interactions.

Our findings that Trp is responsible for PrP−PrP interactions in the absence of metal also support Zahn's proposition that the HGGGW loop conformation promotes PrP aggregation (*33*). We used molecular modeling to explore the possibility of Trp−Trp interactions being the basis for a low level of PrP−PrP interactions observed in the absence of Zn^{2+} or Cu^{2+}. Two noteworthy points from this simulation are (1) the dimer remains intact and (2) a number of Trp residues migrate close to one another, forming what appears to be a hydrophobic cluster. Interestingly, mutation of a single Trp, in this case Trp73, to an Ala causes a noticeable decrease in the percent interaction with no metal present (5.6% in the native PrP model vs 3.4% in the Trp73 → Ala model peptide). Combined, these results support the hypoth-

esis that the Trp residues of the metal binding region are responsible for metal-free PrP−PrP interactions. These interactions may explain the baseline degree of PrP endocytosis observed in the absence of added metals (*8*, *47*). It is interesting to speculate that the hydrophobic clustering of tryptophans may also be the basis of irreversible aggregation when the octarepeat domain is expanded, as found by Leliveld et al. (*23*) and observed in certain fCJD cases (*24*). Analysis of these interactions and the nature of the PrP−PrP structures formed may provide a target for drug design.

The distribution and behavior of GPI-anchored PrP^C on the cell surface is increasingly being regarded as a key to understanding the normal cell biology of PrP^C and perhaps the pathogenesis of TSEs. So far, Cu^{2+}- and Zn^{2+}-stimulated PrP endocytosis is the only well-established physiological response with which this protein is associated. Thus, understanding the mechanisms involved in endocytosis is greatly important. PrP^C has been shown to reside primarily in detergent-insoluble lipid rafts on the surface of neuronal cells, regions reportedly rich in cholesterol and glycosphingolipids (*28*, *48*, *49*). Exposure to Cu^{2+}, and presumably Zn^{2+}, causes PrP^C to move out of the rafts into detergent-soluble regions before it is endocytosed via clathrin-coated pits. Taylor et al. (*49*) argue that Cu^{2+} binding lowers PrP^C's affinity for unspecified raft components, thus freeing PrP^C so it can dissociate from the raft domain and then be internalized. Our findings here, that Cu^{2+} and Zn^{2+} cause PrP to self-associate, provide a plausible mechanism for this proposal. Alternatively, the self-association of PrP may give the newly formed oligomers the ability to exit the raft domain, a proposal similar in nature to that of Zahn, where pH-dependent aggregation of PrP^C molecules within lipid rafts may concentrate the protein sufficiently to stimulate endocytosis [although in this case no reference was made to Cu^{2+} stimulating endocytosis (*33*)]. Whatever the case may be, PrP dimers or oligomers are sure to play an important role in Cu^{2+}- and Zn^{2+}-stimulated endocytosis.

ACKNOWLEDGMENT

We thank Toby Allen for his advice and use of his HPLC system, Allison Danell for her counsel and assistance with mass spectrometry, and Yumin Li for her assistance with graphics.

REFERENCES

1. Prusiner, S. B. (1998) Prions, *Proc. Natl. Acad. Sci. U.S.A. 95*, 13363−13383.
2. Wopfner, F., Weidenhofer, G., Schneider, R., von Brunn, A., Gilch, S., Schwarz, T. F., Werner, T., and Schatzl, M. (1999) Analysis of 27 mammalian and 9 avian PrPs reveals high conservation of flexible regions of the prion protein, *J. Mol. Biol. 289*, 1163−1178.
3. Bueler, H., Fischer, M., Lang, Y., Bluethmann, H., Lipp, H. P., Dearmond, S. J., Prusiner, S. B., Aguet, M., and Weissmann, C. (1992) Normal Development and Behavior of Mice Lacking the Neuronal Cell-Surface Prp Protein, *Nature 356*, 577−582.
4. Brown, D. R., Qin, K. F., Herms, J. W., Madlung, A., Manson, J., Strome, R., Fraser, P. E., Kruck, T., vonBohlen, A., SchulzSchaeffer, W., Giese, A., Westaway, D., and Kretzschmar, H. (1997) The cellular prion protein binds copper in vivo, *Nature 390*, 684−687.
5. Klamt, F., Dal-Pizzol, F., da Frota, M. L. C., Walz, R., Andrades, M. E., da Silva, E. G., Brentani, R. R., Izquierdo, I., and Moreira, J. C. F. (2001) Imbalance of antioxidant defense in mice lacking cellular prion protein, *Free Radical Biol. Med. 30*, 1137−1144.
6. Estibeiro, J. P. (1996) Multiple roles for PrP in the prion diseases, *Trends Neurosci. 19*, 257−258.
7. Prusiner, S. B. (1997) Prion diseases and the BSE crisis, *Science 278*, 245−251.
8. Pauly, P. C., and Harris, D. A. (1998) Copper stimulates endocytosis of the prion protein, *J. Biol. Chem. 273*, 33107−33110.
9. Brown, L. R., and Harris, D. A. (2003) Copper and zinc cause delivery of the prion protein from the plasma membrane to a subset of early endosomes and the Golgi, *J. Neurochem. 87*, 353−363.
10. Brown, D. R., Wong, B. S., Hafiz, F., Clive, C., Haswell, S. J., and Jones, I. M. (1999) Normal prion protein has an activity like that of superoxide dismutase, *Biochem. J. 344*, 1−5.
11. Burns, C. S., Aronoff-Spencer, E., Dunham, C. M., Lario, P., Avdievich, N. I., Antholine, W. E., Olmstead, M. M., Vrielink, A., Gerfen, G. J., Peisach, J., Scott, W. G., and Millhauser, G. L. (2002) Molecular features of the copper binding sites in the octarepeat domain of the prion protein, *Biochemistry 41*, 3991−4001.
12. Rachidi, W., Vilette, D., Guiraud, P., Arlotto, M., Riondel, J., Laude, H., Lehmann, S., and Favier, A. (2003) Expression of prion protein increases cellular copper binding and antioxidant enzyme activities but not copper delivery, *J. Biol. Chem. 278*, 9064−9072.
13. Mouillet-Richard, S., Ermonval, M., Chebassier, C., Laplanche, J. L., Lehmann, S., Launay, J. M., and Kellermann, O. (2000) Signal transduction through prion protein, *Science 289*, 1925−1928.
14. Mange, A., Milhavet, O., Umlauf, D., Harris, D., and Lehmann, S. (2002) PrP-dependent cell adhesion in N2a neuroblastoma cells, *FEBS Lett. 514*, 159−162.
15. Bounhar, Y., Zhang, Y., Goodyer, C. G., and LeBlanc, A. (2001) Prion protein protects human neurons against Bax-mediated apoptosis, *J. Biol. Chem. 276*, 39145−39149.
16. Qin, K. F., Yang, Y., Mastrangelo, P., and Westaway, D. (2002) Mapping Cu(II) binding sites in prion proteins by diethyl pyrocarbonate modification and matrix-assisted laser desorption ionization-time of flight (MALDI-TOF) mass spectrometric footprinting, *J. Biol. Chem. 277*, 1981−1990.
17. Kramer, M. L., Kratzin, H. D., Schmidt, B., Romer, A., Windl, O., Liemann, S., Hornemann, S., and Kretzschmar, H. (2001) Prion protein binds copper within the physiological concentration range, *J. Biol. Chem. 276*, 16711−16719.
18. Burns, C. S., Aronoff-Spencer, E., Legname, G., Prusiner, S. B., Antholine, W. E., Gerfen, G. J., Peisach, J., and Millhauser, G. L. (2003) Copper coordination in the full-length, recombinant prion protein, *Biochemistry 42*, 6794−6803.
19. Chattopadhyay, M., Walter, E. D., Newell, D. J., Jackson, P. J., Aronoff-Spencer, E., Peisach, J., Gerfen, G. J., Bennett, B., Antholine, W. E., and Millhauser, G. L. (2005) The octarepeat domain of the prion protein binds Cu(II) with three distinct coordination modes at pH 7.4, *J. Am. Chem. Soc. 127*, 12647−12656.
20. Morante, S., Gonzalez-Iglesias, R., Potrich, C., Meneghini, C., Meyer-Klaucke, W., Menestrina, G., and Gasset, M. (2004) Inter- and intra-octarepeat Cu(II) site geometries in the prion protein: Implications in Cu(II) binding cooperativity and Cu(II)-mediated assemblies, *J. Biol. Chem. 279*, 11753−11759.
21. Sumudhu, W., Perera, S., and Hooper, N. M. (2001) Ablation of the metal ion-induced endocytosis of the prion protein by disease-associated mutation of the octarepeat region, *Curr. Biol. 11*, 519−523.
22. Sakudo, A., Lee, D. C., Saeki, K., Nakamura, Y., Inoue, K., Matsumoto, Y., Itohara, S., and Onodera, T. (2003) Impairment of superoxide dismutase activation by N-terminally truncated prion protein (PrP) in PrP-deficient neuronal cell line, *Biochem. Biophys. Res. Commun. 308*, 660−667.
23. Leliveld, S. R., Dame, R. T., Wuite, G. J. L., Stitz, L., and Korth, C. (2006) The expanded octarepeat domain selectively binds prions and disrupts homomeric prion protein interactions, *J. Biol. Chem. 281*, 3268−3275.
24. Goldfarb, L. G., Brown, P., McCombie, W. R., Goldgaber, D., Swergold, G. D., Wills, P. R., Cervenakova, L., Baron, H., Gibbs, C. J., and Gajdusek, D. C. (1991) Transmissible Familial Creutzfeldt-Jakob Disease Associated with 5, 7, and 8 Extra Octapeptide Coding Repeats in the Prnp Gene, *Proc. Natl. Acad. Sci. U.S.A. 88*, 10926−10930.
25. Gonzalez-Iglesias, R., Elvira, G., Rodriguez-Navarro, J. A., Velez, M., Calero, M., Pajares, M. A., and Gasset, M. (2004) Cu^{2+}

binding triggers α BoPrP assembly into insoluble laminar polymers, *FEBS Lett. 556*, 161−166.
26. Caughey, B., and Raymond, G. J. (1991) The Scrapie-Associated Form of Prp Is Made from a Cell-Surface Precursor that Is both Protease-Sensitive and Phospholipase-Sensitive, *J. Biol. Chem. 266*, 18217−18223.
27. Borchelt, D. R., Taraboulos, A., and Prusiner, S. B. (1992) Evidence for Synthesis of Scrapie Prion Proteins in the Endocytic Pathway, *J. Biol. Chem. 267*, 16188−16199.
28. Vey, M., Pilkuhn, S., Wille, H., Nixon, R., Dearmond, S. J., Smart, E. J., Anderson, R. G. W., Taraboulos, A., and Prusiner, S. B. (1996) Subcellular colocalization of the cellular and scrapie prion proteins in caveolae-like membranous domains, *Proc. Natl. Acad. Sci. U.S.A. 93*, 14945−14949.
29. Hicks, M. R., Gill, A. C., Bath, I. K., Rullay, A. K., Sylvester, I. D., Crout, D. H., and Pinheiro, T. J. T. (2006) Synthesis and structural characterization of a mimetic membrane-anchored prion protein, *FEBS Lett. 273*, 1285−1299.
30. Eberl, H., Tittmann, P., and Glockshuber, R. (2004) Characterization of recombinant, membrane-attached full-length prion protein, *J. Biol. Chem. 279*, 25058−25065.
31. Ma, L., Morgan, J. C., Stancill, W. E., and Allen, W. E. (2004) Phosphorylated 1,6-diphenyl-1,3,5-hexatriene, *Bioorg. Med. Chem. Lett. 14*, 1075−1078.
32. Case, D. A., Darden, T. A., Cheatham, T. E., III, Simmerling, C. L., Wang, J., Duke, R. E., Luo, R., Wang, K. M. M. B., Pearlman, D. A., Crowley, M., Brozell, S., Tsui, V., Gohlke, H., Mongan, J., Cui, V. H. G., Beroza, P., Schafmeister, C., Caldwell, J. W., Ross, W. S., and Kollman, P. A. (2004) *AMBER 8*, University of California, San Francisco.
33. Zahn, R. (2003) The octapeptide repeats in mammalian prion protein constitute a pH-dependent folding and aggregation site, *J. Mol. Biol. 334*, 477−488.
34. Whittal, R. M., Ball, H. L., Cohen, F. E., Burlingame, A. L., Prusiner, S. B., and Baldwin, M. A. (2000) Copper binding to octarepeat peptides of the prion protein monitored by mass spectrometry, *Protein Sci. 9*, 332−343.
35. Jackson, G. S., Murray, I., Hosszu, L. L. P., Gibbs, N., Waltho, J. P., Clarke, A. R., and Collinge, J. (2001) Location and properties of metal-binding sites on the human prion protein, *Proc. Natl. Acad. Sci. U.S.A. 98*, 8531−8535.
36. Watt, N. T., and Hooper, N. M. (2003) The prion protein and neuronal zinc homeostasis, *Trends Biochem. Sci. 28*, 406−410.
37. Lovell, M. A., Robertson, J. D., Teesdale, W. J., Campbell, J. L., and Markesbery, W. R. (1998) Copper, iron and zinc in Alzheimer's disease senile plaques, *J. Neurol. Sci. 158*, 47−52.
38. Frederickson, C. J., Rampy, B. A., Reamyrampy, S., and Howell, G. A. (1992) Distribution of Histochemically Reactive Zinc in the Forebrain of the Rat, *J. Chem. Neuroanat. 5*, 521−530.
39. Hershey, C. O., Hershey, L. A., Varnes, A., Vibhakar, S. D., Lavin, P., and Strain, W. H. (1983) Cerebrospinal-Fluid Trace-Element Content in Dementia: Clinical, Radiologic, and Pathologic Correlations, *Neurology 33*, 1350−1353.
40. Frederickson, C. J., Giblin, L. J., Krezel, A., McAdoo, D. J., Muelle, R. N., Zeng, Y., Balaji, R. V., Masalha, R., Thompson, R. B., Fierke, C. A., Sarvey, J. M., de Valdenebro, M., Prough, D. S., and Zornow, M. H. (2006) Concentrations of extracellular free zinc (pZn)(e) in the central nervous system during simple anesthetization, ischemia and reperfusion, *Exp. Neurol. 198*, 285−293.
41. Assaf, S. Y., and Chung, S. H. (1984) Release of Endogenous Zn^{2+} from Brain Tissue during Activity, *Nature 308*, 734−736.
42. Berg, J. M., and Shi, Y. G. (1996) The galvanization of biology: A growing appreciation for the roles of zinc, *Science 271*, 1081−1085.
43. Chlebowski, J. F. C. J. E. (1976) in *Metal Ions in Biological Systems* (Siegel, H., Ed.) pp 2−124, Marcel Dekker, New York.
44. Michelitsch, M. D., and Weissman, J. S. (2000) A census of glutamine/asparagine-rich regions: Implications for their conserved function and the prediction of novel prions, *Proc. Natl. Acad. Sci. U.S.A. 97*, 11910−11915.
45. Perutz, M. F., Staden, R., Moens, L., and Debaere, I. (1993) Polar Zippers, *Curr. Biol. 3*, 249−253.
46. Perutz, M. F., Johnson, T., Suzuki, M., and Finch, J. T. (1994) Glutamine Repeats as Polar Zippers: Their Possible Role in Inherited Neurodegenerative Diseases, *Proc. Natl. Acad. Sci. U.S.A. 91*, 5355−5358.
47. Shyng, S. L., Huber, M. T., and Harris, D. A. (1993) A Prion Protein Cycles between the Cell Surface and an Endocytic Compartment in Cultured Neuroblastoma Cells, *J. Biol. Chem. 268*, 15922−15928.
48. Gorodinsky, A., and Harris, D. A. (1995) Glycolipid-Anchored Proteins in Neuroblastoma Cells Form Detergent-Resistant Complexes without Caveolin, *J. Cell Biol. 129*, 619−627.
49. Taylor, D. R., Watt, N. T., Perera, W. S. S., and Hooper, N. M. (2005) Assigning functions to distinct regions of the N-terminus of the prion protein that are involved in its copper-stimulated, clathrin-dependent endocytosis, *J. Cell Sci. 118*, 5141−5153.

BI602473R